

# On the reliability of Stokes diagnostics of magnetic elements away from solar disc centre

S.K. Solanki<sup>1</sup>, O. Steiner<sup>2,3</sup>, M. Bünte<sup>1</sup>, G. Murphy<sup>4</sup>, and S.R.O. Ploner<sup>1</sup>

<sup>1</sup> Institute of Astronomy, ETH-Zentrum, CH-8092 Zürich, Switzerland

<sup>2</sup> Kiepenheuer Institut für Sonnenphysik, Schöneckstrasse 6, D-79104 Freiburg i.Br., Germany

<sup>3</sup> High Altitude Observatory, National Center for Atmospheric Research, Boulder, CO 80307, USA

<sup>4</sup> Applied Physics Laboratory, Johns Hopkins University, Laurel, MD 20702, USA

Received 16 June 1997 / Accepted 22 December 1997

**Abstract.** The spectropolarimetric signature of models of small-scale magnetic features is well understood at the centre of the solar disc, but has been little studied near the solar limb, mainly because the detailed geometry of the flux tubes must then be taken into account in a realistic analysis. We present multi-ray calculations of Stokes profiles through arrays of 2-D magnetohydrostatic models of small flux tubes. We compare the Stokes profile shapes and Stokes based diagnostics ( $Q$  to  $V$  ratio,  $V$  amplitude, magnetic line ratio, centre of gravity wavelengths, etc.) resulting from plane-parallel and 2-D flux-tube models at different limb distances for two lines in the visible and an infrared H-band line. For the visible lines around 5250 Å all the diagnostics we have studied, with the exception of the  $Q$  and  $U$  to  $V$  ratio, are significantly affected by the finite size of the flux tubes and the passage of the rays through non-magnetic material near the limb. We show that magnetic filling factors and the global magnetic flux may be underestimated using the usual calibration techniques. In addition, near the solar limb the magnetic line ratio can move into a regime that is forbidden according to simpler models. The spatially averaged longitudinal field derived from the centre-of-gravity method also becomes strongly model dependent. The thermal structure of the non-magnetic atmosphere appears to play a particularly important role in determining the values of these diagnostic parameters. The infrared line at 1.5648  $\mu\text{m}$ , on the one hand, reacts little to the external atmosphere and provides superior diagnostics of both the magnetic field strength and filling factor. On the other hand, for a flux tube with a sharp boundary this line shows little dependence on the flux-tube diameter, in contrast to the earlier findings of Zayer et al. (1989).

**Key words:** Sun: magnetic fields – Sun: infrared – Sun: faculae, plagues – polarization – line: profiles – line: formation – radiative transfer

## 1. Introduction

A number of spectropolarimetric diagnostics have been developed specifically to study the structure and dynamics of small magnetic flux tubes that are observed in the photospheric layers of the solar atmosphere (see Solanki 1993 for a detailed review). Most of these diagnostics have been developed and tested for vertically incident lines of sight only, corresponding to observations at the centre of the solar disc. The present paper is intended to study the utility of some of these diagnostics for observations outside disc centre.

One reason why most Stokes diagnostics have been tested only under conditions pertaining to the centre of the solar disc is that away from disc centre the geometry of the magnetic feature plays a significant role. At the centre of the solar disc (i.e. at  $\mu = \cos \theta = 1$ , where  $\theta$  is the heliocentric angle), the geometry of a vertical flux tube, i.e. its finite width, cross-sectional shape and area as a function of height, usually does not affect observations (see, e.g., Steiner & Pizzo 1989; Solanki 1989; Keller et al. 1990). Exceptions are any Stokes  $V$  asymmetry produced by flows outside the flux tubes (Grossmann-Doerth et al. 1988; Solanki 1989), strongly split lines in the infrared (Zayer et al. 1989; Solanki et al. 1992; Bruls & Solanki 1994) and investigations aiming at the study of magnetic canopies or the upper photosphere / lower chromosphere in general (Solanki et al. 1991; Faurobert-Scholl 1992, 1994; Briand & Solanki 1995).

The reason for the unimportance of the flux-tube geometry at  $\mu = 1$  is the alignment of the flux tube axis with the line of sight. At  $\mu = 1$  the dominant fraction of the polarized radiation comes from rays that stay completely within the flux tube in the visible layers, while only a minor portion pierces the flux tube boundary (Solanki 1989).

The situation changes completely when moving away from  $\mu = 1$ . Every ray then passes through both strong flux-tube magnetic field and intermediate field-free plasma, so that the size and shape of the flux tube cannot be ignored any longer. Of the few investigations that take the geometry into account when calculating spectral lines produced by flux tubes viewed at an angle, most have restricted the rays to the central plane, i.e. the plane formed by the flux tube axis and a sightline ray

passing through that axis (e.g. Walton 1987; Zayer et al 1989; Grossmann-Doerth et al. 1989; Steiner et al. 1996, Ploner & Solanki 1997). This plane divides a cylindrical flux tube into two equal halves, as seen by the observer. So far only Bunte et al. (1993) and Audic (1991) have considered Stokes transfer along rays passing through the full, axially symmetric flux tube, including regions outside the central plane.<sup>1</sup> These two investigations differ in their aims. Bunte et al. (1993) were specifically interested in the centre-to-limb variation (CLV) of the Stokes  $V$  asymmetry, while Audic (1991) considered idealized spectral lines resulting from a single model flux tube for a simulated high resolution observation.

The present work is complementary to both of these. We investigate various diagnostics of solar magnetic field strength and inclination, temperature, magnetic filling factor and flux-tube diameter. We lay particular emphasis on the dependence of these diagnostics on the flux-tube diameter. We restrict ourselves to the currently typical situation of observations that cannot resolve the flux tubes.

## 2. Hydromagnetic model and line transfer

### 2.1. Magnetohydrostatic model

We describe the magnetic structure of the network or an active region plage by a periodic array of rotationally symmetric, vertical flux tubes in magnetohydrostatic (MHS) equilibrium. They are embedded in a static field-free gas. The magnetic structure is obtained as a numerical solution of the MHS equations for prescribed internal and external stratification of the gas pressure. The procedure is described in detail by Steiner et al. (1986). The radius  $R^*$  of the flux tube at  $z = 0$  (i.e. unit continuum optical depth  $\tau_c$  at 5000 Å in the embedding atmosphere), the filling factor  $f(z = 0) = f^*$  (i.e. the area occupied by the flux-tube magnetic field at  $z = 0$  divided by the total area) and the pressure stratification may be prescribed freely. The vertical component of the magnetic field is kept constant across the flux tube radius at the bottom of the computational box, which then is still true to within a few percent at  $z = 0$ . We have determined the value of the internal gas pressure at  $z = 0$ ,  $p^*$  by prescribing  $B^*$ , the field strength on the flux tube axis at that level. Here we keep  $B^*$  fixed at the typically observed value of 1600 G (e.g., Rüedi et al. 1992). The internal gas pressure stratification is given by the temperature  $T(z)$  of the plage flux-tube model PLA of Solanki (1986) and the condition of hydrostatic equilibrium, while the external atmosphere is described by HSCOOL, which is similar to the HSRA (Gingerich et al. 1971), except that it is cooler by approximately 250 K at all heights. This choice of  $T(z)$  demonstrates the influence of the non-magnetic atmosphere between the flux tubes on the Stokes profiles particularly clearly. The flux-tube models calculated and analyzed during the present investigation are listed in Table 1. For comparison we often use a 1-D plane-parallel atmosphere with data from PLA and with a

<sup>1</sup> Caccin & Severino (1979) and Chapman & Gingell (1984) have also considered rays outside the central plane, but for continuum radiation only.

**Table 1.** Summary of the analyzed magnetohydrostatic models

Model	$B^*$ [G]	$R^*$ [km]	$f^*$ [%]	Dashed pattern used in figures
B	1600	100	5	—————
C	1600	100	10	— — —
D	1600	50	5	. - . - . - . -
E	1600	200	5	- - - - -
G	1600	10	5	. . . - . . . -
PLA	1600	$\infty$	$\infty$	. . . . .

homogeneous, vertical magnetic field  $B(z)$  equal to the values along the flux-tube axis of the other models. It turns out that model C gives results very similar to model B for almost all parameters, except the magnetic line ratio (Sect. 3.5) and is not discussed separately except in that section.

### 2.2. Radiative transfer along multiple rays

The procedure employed to diagnose the hydromagnetic models described in Sect. 2.1 is basically the same as that described by Bunte et al. (1993). To summarize, we first determine the atmospheric quantities required for the radiative transfer of Zeeman split lines along a set of parallel rays inclined to the vertical by a prescribed angle  $\theta$ . The rays pass through a periodic two-dimensional array of identical model flux tubes and are distributed such that the whole set samples a full period of the flux-tube array at a given height. This is appropriate for simulating low spatial resolution observations. Fig. 1 shows outlines of two arrays of flux tubes of different  $R^*$  and the bundle of rays passing through them in the central plane at two different  $\mu$  values each. Note how the number of flux tubes (or flux-tube walls) that a ray crosses depends on both  $\mu$  and the flux-tube radius.

We use  $20 \times 21 (= 410)$  rays in all of the following calculations. We also consider Stokes  $Q$  and  $U$  in addition to Stokes  $V$  and therefore distribute rays over a full period also in the direction perpendicular to the plane of Fig. 1.

We use an adaptive step size grid along each ray. It ensures that the number of grid points along any ray section that pierces a flux tube is larger than some minimum value (recall that the Stokes parameters  $Q$ ,  $U$  and  $V$  obtain constructive contributions only within the magnetized part of the atmosphere) and that a maximum optical step size of  $\Delta \log \tau = 0.1$  is not exceeded, which is important to maintain the sharpness of the flux tube boundary on the optical depth scale.

Once the atmosphere has been computed along each ray, the Stokes parameters are calculated using the radiative transfer code described by Solanki (1987), which, for the solution of the Unno-Rachkovsky equations, now incorporates the Diagonal Element Lambda Operator (DELO) routines of Rees et al. (1989).

We have calculated three spectral lines for each model, Fe I 5250.2 Å, Fe I 5247.1 Å and Fe I 15648 Å, all of which have in the past been extensively used to study solar magnetism. For

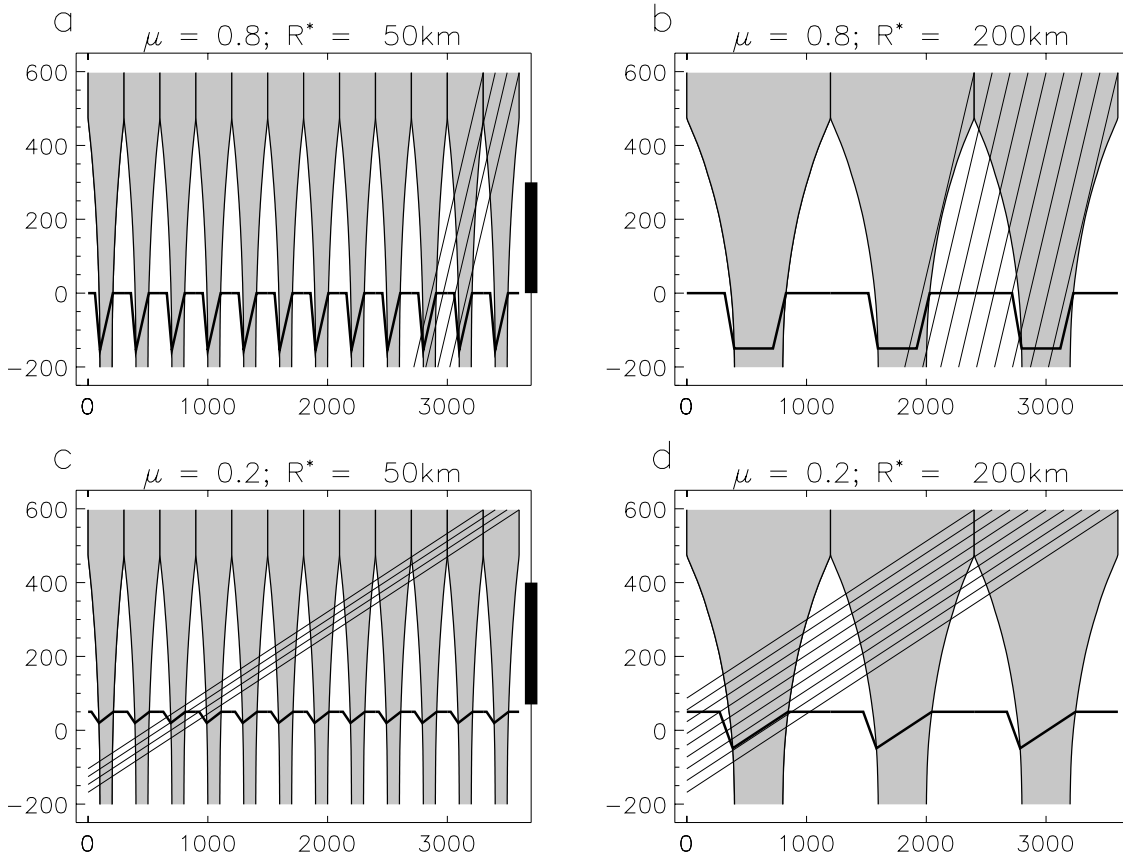


**Fig. 1a–d** Cut along the central plane (i.e. the plane spanned by the flux-tube axis and the line of sight) through arrays of two flux-tube models, showing the flux-tubes shaded), and a sample of rays in the central plane, along which line profiles were calculated. For the line profile calculations more rays were used. The thick line delineates the continuum optical depth unity ( $\tau_c = 1$ ) level at the appropriate viewing angle. The thick vertical bar on the right border frame indicates roughly the height range over which Fe I 5250.2 Å is on average formed. **a** Model D with  $R^* = 50$  km, **b** model E with  $R^* = 200$  km. Profiles are also calculated along rays lying within other planes parallel to the central plane, as described in the text and illustrated by Bünte et al. (1993). The angle  $\theta$  between the rays and the flux-tube axis is the same in both figures, and corresponds to  $\mu = \cos \theta = 0.8$ . **c** and **d** show the same models as Figs. 1a and b, respectively, but now with rays having an inclination corresponding to  $\mu = 0.2$ .

the two visible lines we use the same atomic data as Solanki et al. (1987), while for the infrared line we follow Solanki et al. (1992).

### 3. Results

We discuss the results for the different line parameters and diagnostics individually. The infrared line is discussed separately in Sect. 3.7.

#### 3.1. Profile shapes

The spectral shapes of Stokes  $Q$ ,  $U$  and  $V$  resulting from multi-ray calculations as described in Sect. 2.2, can deviate significantly from profiles calculated in a plane parallel (i.e. 1-D) atmosphere. At  $\mu = \cos \theta = 1$  these differences are minute and the Stokes  $V$  profiles are almost indistinguishable while at  $\mu = 0.2$  their shapes are totally different, with the multi-ray profile having narrow, widely separated lobes and often an inversion

at the line core. Examples of multi-ray  $V$  profiles at  $\mu = 0.2$ , unbroadened by macroturbulence, are shown in Fig. 2a.

The  $V$  lobe separation of the multi-ray profiles, if taken at face value to represent Zeeman splitting, suggests a larger  $B$  at  $\mu = 0.2$  than at  $\mu = 1$ . Such a hypothetical observation could thus be misconstrued to indicate a field strength increasing with height, while exactly the opposite is the case in the underlying model.

To understand the multi-ray profile shape we first note that the inversion in the centre of the  $V$  profile is not due to magneto-optical effects. We confirmed this with calculations that had magneto-optical effects switched off. Next we consider the transfer equations for a Zeeman split spectral line in LTE,

$$\frac{dI_\nu}{d\tau_c} = (1 + \eta_I)(I_\nu - B_\nu) + \eta_Q Q_\nu - \eta_U U_\nu + \eta_V V_\nu, \quad (1)$$

$$\frac{dQ_\nu}{d\tau_c} = \eta_Q(I_\nu - B_\nu) + (1 + \eta_I)Q_\nu + \rho_V U_\nu - \rho_U V_\nu, \quad (2)$$

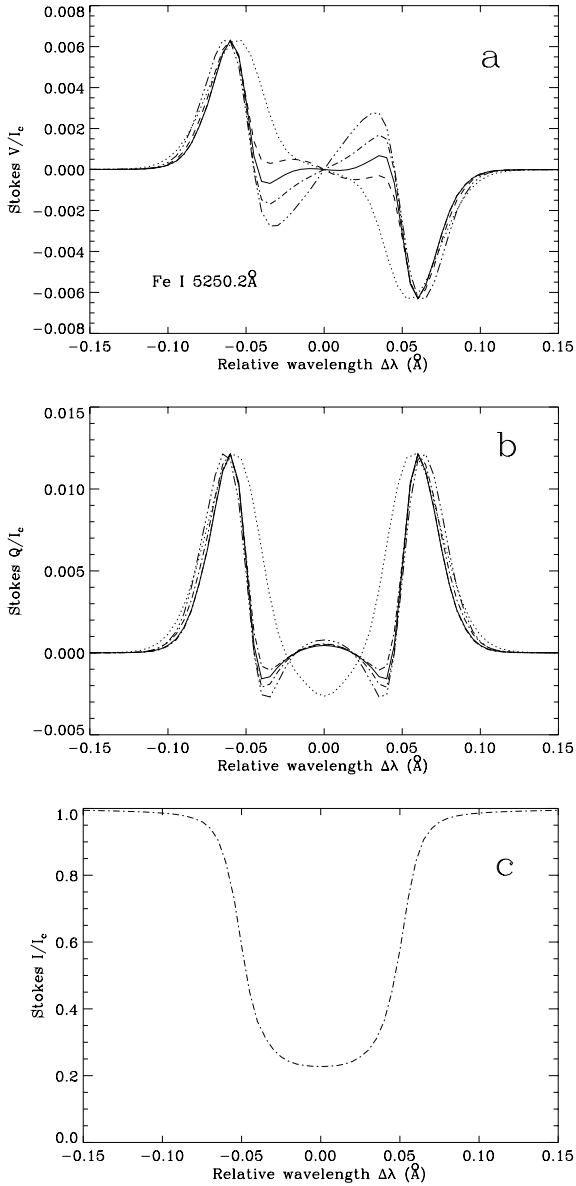


**Fig. 2a–c** Stokes profiles for models B (solid), E (dashed), D (dot-dashed), G (triple dot-dashed) and the plane parallel PLA model (dotted) at  $\mu = \cos \theta = 0.2$ . See also Table 1 for a legend of the line patterns. **a** Stokes  $V$  profiles, **b** Stokes  $Q$  profiles, **c** Stokes  $I$  profile for model D. The  $I$  profiles for the other models are similar in shape, and are not plotted for clarity. All profiles in a given frame are normalized to a single amplitude in order to emphasize differences in shape.

$$\frac{dU_\nu}{d\tau_c} = \eta_U(I_\nu - B_\nu) - \rho_V Q_\nu + (1 + \eta_I)U_\nu + \rho_Q V_\nu, \quad (3)$$

$$\frac{dV_\nu}{d\tau_c} = \eta_V(I_\nu - B_\nu) + \rho_U Q_\nu - \rho_Q U_\nu + (1 + \eta_I)V_\nu. \quad (4)$$

Here  $(I_\nu, Q_\nu, U_\nu, V_\nu)^T$  is the Stokes vector at frequency  $\nu$ ,  $\eta_I, \eta_Q, \eta_U$  and  $\eta_V$  are line absorption coefficients relative to the continuum absorption coefficient,  $\rho_Q, \rho_U$  and  $\rho_V$  are the corresponding magneto-optical coefficients (which in general are considerably smaller than  $\eta_I, \eta_Q$ , etc.),  $B_\nu$  is the Planck

function and  $\tau_c$  is the continuum optical depth along the line of sight. Expressions for  $\eta_I, \eta_Q, \eta_U, \eta_V, \rho_Q, \rho_U$  and  $\rho_V$  are given by, e.g., Landi Degl’Innocenti (1976). Along most rays in the geometry considered here, light enters the flux tube from the field-free atmosphere, in which  $\eta_Q = \eta_U = \eta_V = \rho_Q = \rho_U = \rho_V = 0$ . For simplicity we assume that the magnetic filling factor of the unresolved flux-tubes is sufficiently small, so that always  $V, Q, U \ll I$ . This condition is fulfilled by most observations in the quiet sun and in solar plages ( $Q, U, V$  amplitudes typically do not exceed a few percent). For large enough  $\theta$  it is fulfilled along each ray individually, since then a large fraction of it passes through field-free atmosphere. In addition, for lines of sufficient strength, such as the ones we consider,  $\eta_Q, \eta_U, \eta_V \approx O(\eta_I) \gtrsim 1$ . In this case Eqs. (1)–(4) can be simplified to

$$\frac{dI_\nu}{d\tau_c} \approx (1 + \eta_I)(I_\nu - B_\nu), \quad (5)$$

$$\frac{dP_\nu}{d\tau_c} \approx \eta_P(I_\nu - B_\nu), \quad (6)$$

where  $P = Q, U$  and  $V$ , in turn. For a thin flux tube and a sufficiently large  $\theta$  we can write as solution of Eq. (6):

$$P_\nu \approx \eta_P(I_\nu - B_\nu)\Delta\tau_c. \quad (7)$$

(We have made use of the boundary condition  $P_\nu \approx 0$  at the first boundary of the flux tube pierced by the ray.)  $\Delta\tau_c < 0$  is the continuum optical depth step across the flux tube. The sign of  $P_\nu$  depends on  $I_\nu - B_\nu$ , i.e. whether the temperature decreases along the ray towards the observer or not. A temperature inversion, i.e. a flux tube that is hotter than its surroundings, gives  $I_\nu < B_\nu$  and leads to an inversion in  $P_\nu$ .

Our model flux tube is hotter than the non-magnetic atmosphere at equal geometrical height in the middle and upper photosphere. This is in agreement with stationary theoretical models incorporating radiative energy transport (e.g. Grossmann-Doerth et al. 1989; Steiner 1990; Steiner & Stenflo 1990; Knölker et al. 1990; Knölker & Schüssler 1992) and empirical models (e.g. Keller et al. 1990; Bruls & Solanki 1993; Briand & Solanki 1995). Within the flux tubes the spectral line cores, which are formed in these layers, thus sample a region in which  $I_\nu - B_\nu < 0$ , which drives them into emission. If the magnetic filling factor is sufficiently small, however, Stokes  $I$  gets its major contribution outside the flux tubes, where  $I_\nu > B_\nu$ , so that a pure absorption profile results, as shown in Fig 2c. Stokes  $Q, U, V$ , on the other hand, obtain their constructive contributions only within the flux tube, with  $B_\nu > I_\nu$  in the upper layers, which leads to the inversions seen in Figs. 2a and b. In summary, at small  $\mu$  the sign of  $V, Q, U$  in the line core depends on the temperature of the flux tube relative to its surroundings for all but the weakest lines.

In either of the considered geometries another effect, first pointed out by Audic (1991), also plays an important role. The polarized signal in the line core is greatly reduced due to absorption in the gas between the flux tube (or the magnetic central

layer) and the observer. There, the transfer equations for polarized light are simply:

$$\frac{dI_\nu}{d\tau_c} = (1 + \eta_I)(I_\nu - B_\nu), \quad (8)$$

$$\frac{dP_\nu}{d\tau_c} = (1 + \eta_I)P_\nu. \quad (9)$$

The solution to Eq. (9) reads

$$P_\nu = P_{0\nu} \exp\left(-\int (1 + \eta_I) d\tau'_c\right). \quad (10)$$

Inserting  $P_{0\nu}$  from Eq. (7) we obtain

$$P_\nu \approx \eta_P (I_{0\nu} - B_{0\nu}) \Delta\tau_c \exp\left(-\int (1 + \eta_I) d\tau'_c\right), \quad (11)$$

where  $I_{0\nu}$  and  $B_{0\nu}$  are the intensity and source function referring to the portion of the ray within the flux tube.

This effect tends to make  $Q$ ,  $U$ ,  $V$  largest in the line wing (where  $1 + \eta_I$  is small) and gives them flat cores (where  $1 + \eta_I$  is large), i.e. it decreases the  $\pi$ - and (to a lesser extent) the  $\sigma$ -peaks and moves the  $\sigma$ -maxima away from the line core (Audic 1991). Again, this effect strongly depends on the thermal structure of the non-magnetic atmosphere, through the temperature dependence of  $\eta_I$  (e.g. the  $\eta_I$  of low excitation Fe I lines increases with decreasing temperature). Both effects, the inversion and the absorption at the line core increase the Stokes  $V$  lobe separation and therefore lead to an unexpected increase of that measure with decreasing  $\mu$ .

### 3.2. Shapes of turbulence-broadened profiles

Consider briefly the influence of a macroturbulent velocity on the Stokes profiles. Such a source of line broadening is generally employed to reproduce the widths and shapes of Stokes profiles (e.g. Solanki 1986; Bünte et al. 1993). If we broaden the calculated profiles by  $2 \text{ km s}^{-1}$ , a value typically required to reproduce observed profiles, then the Stokes profiles of Fig. 2 are transformed into the corresponding profiles plotted in Fig. 3. Note that only the extreme profile produced by model G still shows a significant central inversion after broadening. The Stokes  $V$  profiles show large variations from one model to the next, whereas the  $Q$  profiles of all the models are very similar. Consequently, the variation in flux tube diameter is only distinguishable in Stokes  $V$ , if at all.

It has recently been proposed by Sánchez Almeida et al. (1996) that magnetic elements with sizes even smaller than model G exist (so called MISMAS). Fig. 3a suggests that if these are significantly hotter than their surroundings at the solar limb they should produce  $V$  profiles with strong inversions in their cores. The Stokes  $V$  observations by Stenflo et al. (1987) do not exhibit any significant inversions, suggesting that either the magnetic elements have diameters larger than approximately 50 km or are at roughly the same temperature as the ambient medium. However, a much larger set of observations close to the limb is required to settle this point.

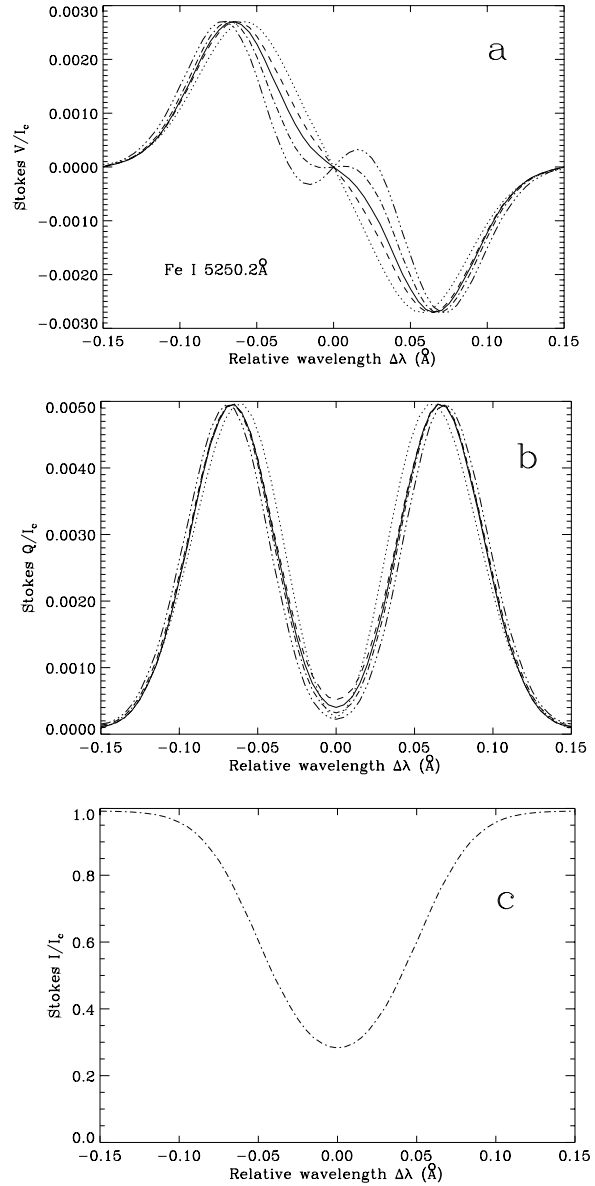


**Fig. 3a–c** Stokes profiles broadened by a macroturbulent velocity of  $2 \text{ km s}^{-1}$  for the same models as in Fig. 2. **a** Stokes  $V$ , **b** Stokes  $Q$ , **c** Stokes  $I$ .

### 3.3. Stokes $Q/V$ ratio and the magnetic inclination angle

The ratio  $\sqrt{Q^2 + U^2}/V$ , usually taken at a fixed wavelength, is a measure of the inclination angle  $\gamma$  of the magnetic vector relative to the line-of-sight. In the past  $\gamma$  has been determined from a plane-parallel, 1-D model with either a height dependent or homogeneous magnetic field (e.g. Ronan et al. 1987; Lites & Skumanich 1990; Lites et al. 1993; Bernasconi et al. 1995; Martínez Pillet et al. 1997). Here we test the accuracy of this approximation by comparing the results of a plane-parallel model with our multi-ray calculations. We note the value of  $Q_{\max}/V_{\max}$  produced for a given 2-D model and then search for the angle  $\gamma$  that gives the same  $Q_{\max}/V_{\max}$  ratio, using the plane-parallel 1-D model PLA. Here  $Q_{\max}$  and  $V_{\max}$  signify

the  $Q$  and  $V$   $\sigma$ -amplitudes, respectively. Our tests are restricted in the sense that we consider only vertical 2-D flux tubes, but we nevertheless test at different  $\gamma = \theta$  values. Since the azimuthal angle  $\chi = 0$ , Stokes  $U$  is not required for this test (although, due to magneto-optical effects, it is generally non-zero).

The estimated error in  $\gamma$  introduced through approximating a flux tube by a plane-parallel atmosphere is on average only  $1.4^\circ$ , with the largest error found by us being  $4^\circ$ . We also find that for all models and spectral lines the errors are largest either closest to the limb ( $\mu = 0.2$ ), or closest to disc centre ( $\mu = 0.8$ ).

In summary, for the determination of the magnetic inclination only, it is quite sufficient to employ a plane parallel model for spatially unresolved observations of a rotationally symmetric magnetic flux tube. Note that, however, if either the spatial resolution element of the spectroscopic observation is much smaller than the flux tube diameter, or the magnetic flux is concentrated into a sheet-like structure (magnetic flux sheet) then the  $Q/V$  ratio is non-vanishing even at disc centre for a perfectly vertical, symmetric structure, thereby falsely suggesting a non-vanishing inclination.

#### 3.4. Centre-to-limb variation of the Stokes $V$ amplitude

For an optically thin spectral line formed in a homogeneous, vertical magnetic field the Stokes  $V$  amplitude scales with  $\cos \gamma$  and thus to first order with  $\mu$ . In a plane-parallel model of a flux tube (with the magnetic field decreasing with height as in our model PLA) there are two effects acting to produce departures from this behaviour. On the one hand the decrease of  $B$  with  $z$  lowers  $V_{\max}$  near the limb for incompletely split lines like  $\lambda 5247.1 \text{ \AA}$  and  $\lambda 5250.2 \text{ \AA}$  since they are formed higher in the atmosphere at small  $\mu$ . On the other hand, due to the thermal structure of, e.g., the plage flux-tube model, these temperature sensitive lines, and thus their  $V_{\max}$ , are considerably enhanced with decreasing  $\mu$ . The numerical results for  $\lambda 5250.2 \text{ \AA}$ , plotted as the dotted curve in Fig. 4a, show that for a plane-parallel model the latter effect is the dominant one (the dotted curve varies less rapidly than  $\mu$ ). The curves for the multi-ray models lie below the plane-parallel results for sufficiently small  $\mu$ . Also, they strongly differ from each other at intermediate  $\mu$ .

Van Ballegoijen (1985) first proposed that when observing at an angle to the axis of an isolated thin flux tube the  $V$  amplitude should be much lower than in the plane-parallel case. In his calculations Stokes  $V$  at a fixed wavelength drops by a factor of over 10 at  $\mu = 0.8$  for a vertical flux tube with a diameter of 15 km. We qualitatively confirm his result, but find a much gentler drop in  $V_{\max}$  with decreasing  $\mu$  than he did. This is the case even for our model G with  $R^* = 10 \text{ km}$ , comparable with the  $R^*$  of 7.5 km for Van Ballegoijen's model.

At large  $\mu$  one important difference between his and our models is that our flux tubes expand with height, whereas he considered straight flux sheets. At small  $\mu$ , however, the dominant reason for the discrepancy between Van Ballegoijen's and our results is that he considered only a single flux tube and not a whole array. In order to understand that, let us consider a bundle of rays equally distributed over a period of the flux tube array

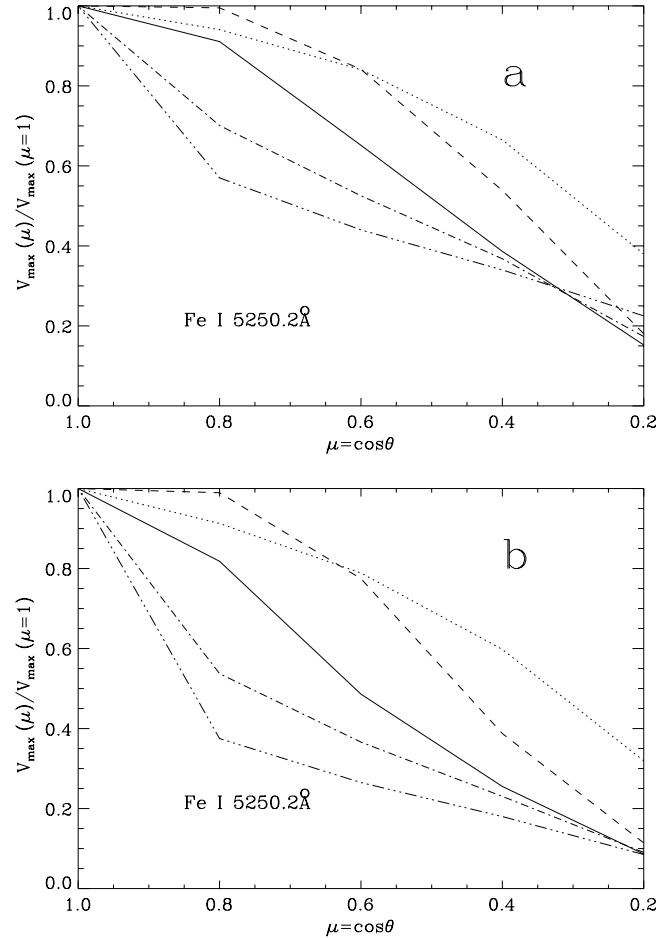


**Fig. 4a and b** Stokes  $V$  amplitude of Fe I 5250.2  $\text{\AA}$  normalized to its value at the centre of the solar disc,  $V_{\max}(\mu)/V_{\max}(\mu = 1)$ , vs.  $\mu$ . Plotted are curves for models B, D, E, G and PLA. The line patterns are identified in Table 1. **a** Amplitude of raw profiles, **b** amplitude of profiles broadened by a macroturbulent velocity of  $2 \text{ km s}^{-1}$ .

as shown in Fig. 1. Then, with increasing inclination (decreasing  $\mu$ ) an increasing number of rays passes at some height in the atmosphere through one or more flux tubes, so that, loosely speaking, the ‘effective’ magnetic filling factor increases with inclination *relative to the case of a single flux tube*, although it does not increase in an absolute sense. We expect that at least in active region plages and the enhanced network a periodic collection of flux tubes, like we model here, comes closer to reality than in a single, isolated flux tube. Consequently, although the effect pointed out by Van Ballegoijen (1985) is present, it is expected to be of smaller magnitude in active regions and the network than his calculations suggested. The response of isolated flux tubes may well be more in accordance with the calculations of Van Ballegoijen (1985).

We attribute the enhanced  $V_{\max}$  of model E at  $\mu = 0.8$  relative to the plane-parallel case to the hot wall present below the external  $\tau = 1$  level in the 2-D MHS models, which becomes increasingly visible as one moves away from disc centre (e.g. Spruit 1976; Knölker & Schüssler 1988). Due to the large continuum intensity resulting from the hot wall the  $V$  profiles

formed along rays piercing it are greatly enhanced in amplitude. On the other hand, below a certain  $\mu$  rays piercing the flux tube wall mainly lie outside the flux tube, so that Stokes  $V$  is small along such rays (partly due to the effects described in Sect. 3.1.). Thus, we expect that there is an intermediate  $\mu$  value at which the visibility of the wall is largest, in which case the rays passing through the hot wall just manage to stay within the flux tube.

In this picture the maximum hot-wall-induced  $V_{\max}$  enhancement happens at increasingly smaller  $\mu$  for increasingly large flux tubes. A comparison of Fig. 1a with 1b shows that whereas all the rays passing through the hot wall in the thick flux tube lie within the flux tube for all  $\tau_c < 1$ , this is patently not the case for the thinner flux tube, although  $\mu$  is the same in both cases. Hence we expect the enhancement of the  $V$  profiles due to the hot walls of the thinner flux tubes to be largest at  $\mu > 0.8$ , which  $\mu$  region is unfortunately not resolved by our  $\mu$  grid.

The application of a macroturbulence reduces  $V_{\max}(\mu < 1)$  relative to  $V_{\max}(\mu = 1)$  for all models. The  $V_{\max}(\mu)$ , normalized to its disc centre value, is plotted in Fig. 4b for profiles broadened by a macroturbulence of  $2 \text{ km s}^{-1}$ . The effect is larger for narrower flux tubes. Near the limb all of our 2-D models produce  $V_{\max}(5250)$  that are approximately a factor of 2 lower than the simple  $V \sim \mu$  estimate. This effect should be kept in mind when determining fluxes from, e.g., full-disc magnetograms.

In Fig. 5 we plot  $V_{\max}$  of  $5247.1 \text{ \AA}$  vs.  $\mu$  for the same models as in Fig. 4a. Interestingly,  $V_{\max}(5247.1 \text{ \AA})$  decreases more rapidly with decreasing  $\mu$  than  $V_{\max}(5250.2 \text{ \AA})$  for all models. The only difference between the two lines is their differing Landé factors. The larger Zeeman sensitivity of  $5250.2 \text{ \AA}$  relative to  $5247.1 \text{ \AA}$  leads to a greater separation between its  $\sigma$ -components. Consequently, the  $\sigma$ -components are less affected by absorption in the field-free part of the atmosphere and by the temperature enhancement in the flux tube (Sect. 3.1.), compared to the  $5247.1 \text{ \AA}$  line. This weakens  $V_{\max}(5247.1 \text{ \AA})$  relative to  $V_{\max}(5250.2 \text{ \AA})$  at small  $\mu$ , leading to significant and surprising consequences for the ratio between the  $V$  profiles of these two lines (see Sect. 3.5.). The above explanation for the difference between  $V_{\max}(5250)$  and  $V_{\max}(5247)$  vs.  $\mu$  is confirmed by the behaviour of the extremely Zeeman sensitive line at  $15648 \text{ \AA}$  (see Sect. 3.7.).

### 3.5. Magnetic line ratio

The ratio

$$\begin{aligned} \text{MLR} &= \frac{V_{\max}(5250.2 \text{ \AA}) g_{\text{eff}}(5247.1 \text{ \AA})}{V_{\max}(5247.1 \text{ \AA}) g(5250.2 \text{ \AA})} \\ &= \frac{2}{3} \frac{V_{\max}(5250)}{V_{\max}(5247)} \end{aligned} \quad (12)$$

is widely accepted as one of the most powerful diagnostics of the intrinsic magnetic field strength of solar magnetic elements (Stenflo 1973; Stenflo & Harvey 1985) and is sometimes referred to simply as the magnetic line ratio, or MLR for short. For a simple model with a homogeneous magnetic field, as used

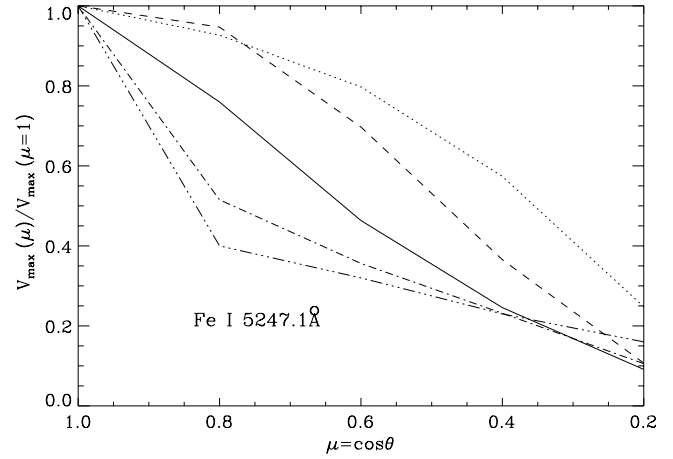


Fig. 5. Same as Fig. 4a for Fe I 5247.1  $\text{\AA}$ .

traditionally to calibrate the MLR, we have  $\text{MLR} \approx 1$  for a sufficiently weak field and  $\text{MLR} < 1$  for stronger fields.

This diagnostic is well studied and understood for longitudinal fields and flux tubes located at  $\mu = 1$ . Its centre-to-limb variation, however, has been studied only for plane-parallel model atmospheres. These showed that for fields inclined to the line of sight the blending and saturation of the  $\pi$ - and  $\sigma$ -components becomes important (Solanki et al. 1987), causing the line ratio to increase with increasing strength of the  $\pi$ -component. For vertical flux tubes this implies that the MLR increases towards the limb. An illustration of this effect is provided by the dotted curve in Fig. 6a, which shows the MLR as a function of  $\mu$  calculated in the plane-parallel PLA atmosphere. A part of its increase towards the solar limb is also due to the decrease of  $B$  with height. The four other curves represent the MLR resulting from multi-ray calculations through models B, C, D and E. At small  $\mu$  all multi-ray models give MLR values greater than unity.<sup>2</sup> Even slightly off disc centre at  $\mu = 0.8$  ( $\theta \approx 35^\circ$ ) one may obtain a MLR of unity which could be misinterpreted as the measurement of an intrinsically weak magnetic field.

MLR values  $> 1$  can be explained using the results of Sects. 3.1. and 3.4. The saturated line core in the field-free part of the atmosphere weakens the  $V$  profile in the core of a sufficiently strong line. As already discussed in Sect. 3.4., the  $V$  lobes of a more strongly Zeeman split line (e.g.  $\lambda 5250.2 \text{ \AA}$ ) lie further from the line core than the  $V$  lobes of a less Zeeman split line (e.g.  $\lambda 5247.1 \text{ \AA}$ ) and are consequently less weakened by transfer effects in the non-magnetic atmosphere. The MLR is thereby increased and exceeds unity in this case.

In order to test this explanation we consider four different, plane-parallel atmospheres with a vertical magnetic field confined to a specific optical depth range only, i.e., a 3-layered model as described in Sect. 3.1:

$$B_z = \begin{cases} 800 \text{ G} & \text{for } \tau_{\min} = 10^{-3} < \tau_{5000} < \tau_{\max} = 10^{-2} \\ 0 & \text{elsewhere} . \end{cases}$$

<sup>2</sup> Note that in Fig. 6a the MLRs for the 2-D models are always larger than for the 1-D model even at  $\mu = 1$ . This is caused by the radial field component in the 2-D models that is absent in the 1-D model.

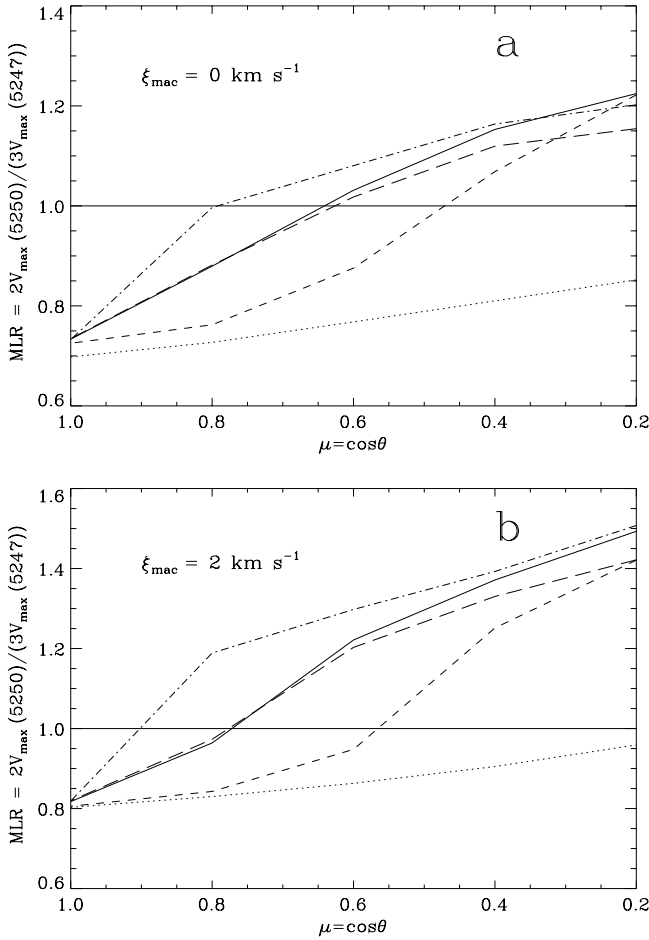


**Fig. 6a and b** Magnetic line ratio (MLR),  $2V_{\max}(5250.2 \text{ \AA}) / 3V_{\max}(5247.1 \text{ \AA})$ , for models B, C, D, E, and PLA (Model C is represented by the long dashes). **a** MLR based on unbroadered profiles, **b** MLR from profiles broadened by a  $2 \text{ km s}^{-1}$  macroturbulence.

**Table 2.** MLR for various plane-parallel models

Test No.	$T(\tau)$ for $B \neq 0$	$T(\tau)$ for $B = 0$	MLR ( $\gamma = 0$ )	MLR ( $\gamma = 80^\circ$ )
1	PLA	PLA	0.79	0.84
2	HSCOOL	HSCOOL	0.90	1.05
3	PLA	HSCOOL	1.15	1.20
4	HSCOOL	PLA	0.73	0.86

In addition, the temperature stratification in the range  $\tau_{\min} < \tau_{5000} < \tau_{\max}$  (i.e. in the central layer) may correspond to a different model atmosphere than that outside this optical depth range. The chosen model combination and the corresponding computed MLR for two different angles  $\gamma$  between the line of sight and the magnetic field are given in Table 2.

As far as line transfer is concerned such an atmosphere composed of 3 horizontal layers, with the (thin) central layer possessing a magnetic field (i.e. it corresponds to the flux tube) and the top and bottom layers being field-free (corresponding to its surroundings), is formally the same as a vertical (thin) flux tube

pierced by an isolated inclined ray. In this simplified geometry we need only consider a vertical ray. In the 3-layer picture a hot flux tube embedded in cool surroundings produces a negative temperature gradient ( $dT/d\tau_c$ ) at the lower boundary of the central layer, while the gradient remains positive at all other heights. Using Eqs. (5) and (7) it is then straightforward to deduce that for a sufficiently thin central layer Stokes  $I$  does not show an inversion in its core, whereas Stokes  $Q$ ,  $U$  and  $V$  do.

Table 2 shows that the MLR is larger for a cooler atmosphere, i.e. for larger line saturation (test No. 2), as compared to the case of a hot atmosphere (test No. 1). Furthermore, it is largest when the magnetic portion is hot and the field-free layers are cool (test No. 3) due to Stokes  $V$  absorption in the field-free gas and the inversion of Stokes  $V$  in the line core (see Sect. 3.1). Note also that the MLR increases with  $\gamma$ . This effect is largest for a low temperature and correspondingly high saturation within the magnetic layer (tests 2 and 4) and it is largely due to blending of the  $\pi$ - and  $\sigma$ -components.

Finally, the MLR becomes even larger if the line profiles are broadened by a macroturbulent velocity (Fig. 6b). In summary, for small magnetic flux tubes the MLR is not a reliable diagnostic for  $B$  too far outside solar disc centre, since it becomes excessively sensitive to the temperature, flux-tube size and turbulent velocity. At present it is not clear from observations whether MLR values greater than unity are present in solar data or not. The few MLR values determined by Stenflo et al. (1987) near the limb all lie below unity, but a larger number of observations are required for a definitive answer.

### 3.6. Centre-of-gravity method

The centre-of-gravity method (or c.g. method) for the longitudinal magnetic flux or filling factor was introduced by Semel (1967). The centre-of-gravity wavelengths  $\lambda_{\pm}$  of the positively and negatively polarized components of a spectral line are defined as:

$$\lambda_{\pm} = \frac{\int (I_c - (I \pm V)) \lambda d\lambda}{\int (I_c - (I \pm V)) d\lambda}. \quad (13)$$

According to the c.g. method the spatially averaged longitudinal magnetic field strength  $\langle B \cos \gamma \rangle$  (in Gauss) is related to  $\lambda_{\pm}$  in a straightforward manner:

$$\langle B \cos \gamma \rangle = \frac{(\lambda_- - \lambda_+)/2}{4.67 \times 10^{-13} \lambda_0^2 g_{\text{eff}}}, \quad (14)$$

with the wavelengths given in  $\text{\AA}$ . Here  $\lambda_0$  is the line centre wavelength and  $g_{\text{eff}}$  is the effective Landé factor.

For an optically thin line Eq. (14) can be shown to be exact for any  $\mu$  or  $\gamma$  value. In plane-parallel atmospheres the accuracy is still high even for optically thick lines (errors  $\lesssim 10\%$ , Semel 1971) and the c.g. technique shows distinct advantages over other techniques for determining  $\langle B \cos \gamma \rangle$  (e.g. Rees & Semel 1979; Grossmann-Doerth et al. 1987; Cauzzi et al. 1993).

This section may be considered to be an extension of the work of Rees & Semel (1979), who based their conclusions on 1.5-D radiative transfer through a vertical flux tube at  $\mu = 1$ .

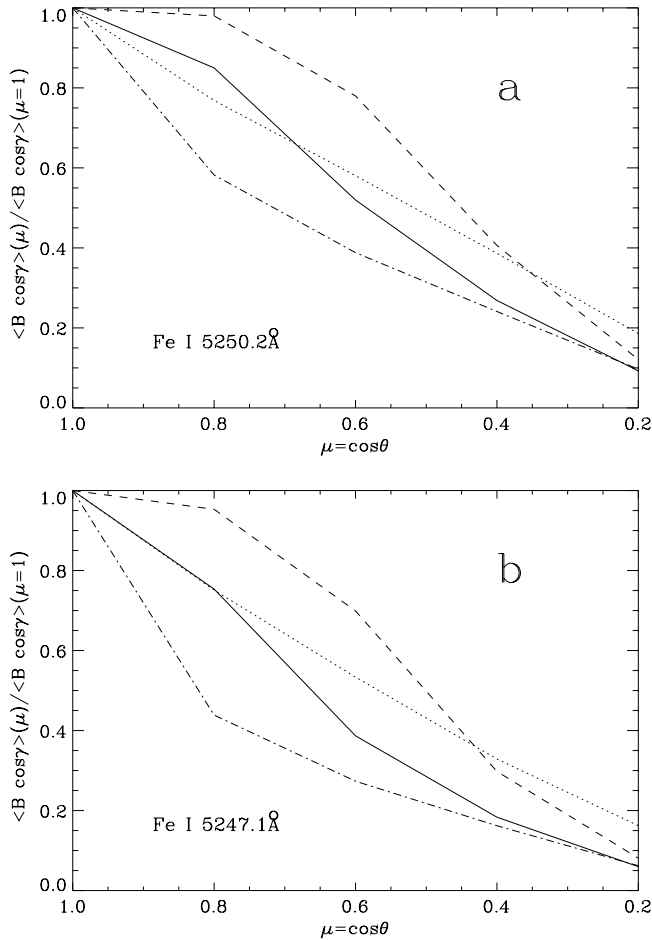


**Fig. 7a and b** Spatially averaged longitudinal field, derived with the centre-of-gravity method, normalized to its value at disc centre,  $\langle B \cos \gamma \rangle(\mu) / \langle B \cos \gamma \rangle(\mu = 1)$  vs.  $\mu$ . Plotted are the results for unbrodened profiles from models B, D, E, and PLA. Macrotrubulence-broadened profiles give practically identical results. **a** Fe I 5250.2 Å, **b** Fe I 5247.1 Å.

In Fig. 7a we plot  $\langle B \cos \gamma \rangle$  derived from Eq. (14), as applied to Fe I 5250.2 Å (the plotted  $\langle B \cos \gamma \rangle$  is normalized to its value at  $\mu = 1$ ). The dotted curve representing the plane-parallel PLA model lies very close to the expected linear dependence on  $\mu$ , confirming the superiority of the c.g. method over the Stokes  $V$  amplitude in this type of model (compare with the dotted curve in Fig. 4a). Unfortunately, the  $\langle B \cos \gamma \rangle$  curves obtained from the 2-D models using the c.g. method are less satisfactory. Thus, for flux tubes  $\langle B \cos \gamma \rangle$  is underestimated by up to a factor of 2 near the limb when diagnosed by the centre-of-gravity method in conjunction with a plane-parallel model. Also, Fe I 5247.1 Å (Fig. 7b) gives consistently lower  $\langle B \cos \gamma \rangle$  values near the limb than 5250.2 Å.

The reason for the difference between the  $\langle B \cos \gamma \rangle$  resulting from plane-parallel and 1.5-D calculations lies once again in transfer effects introduced by the field-free medium into the polarized profiles. Note that the  $V$  profiles produced by the 1.5-D calculations not only have lower amplitudes, but also narrower  $V$  lobes, which reduces their  $\lambda_+ - \lambda_-$  additionally. The c.g.

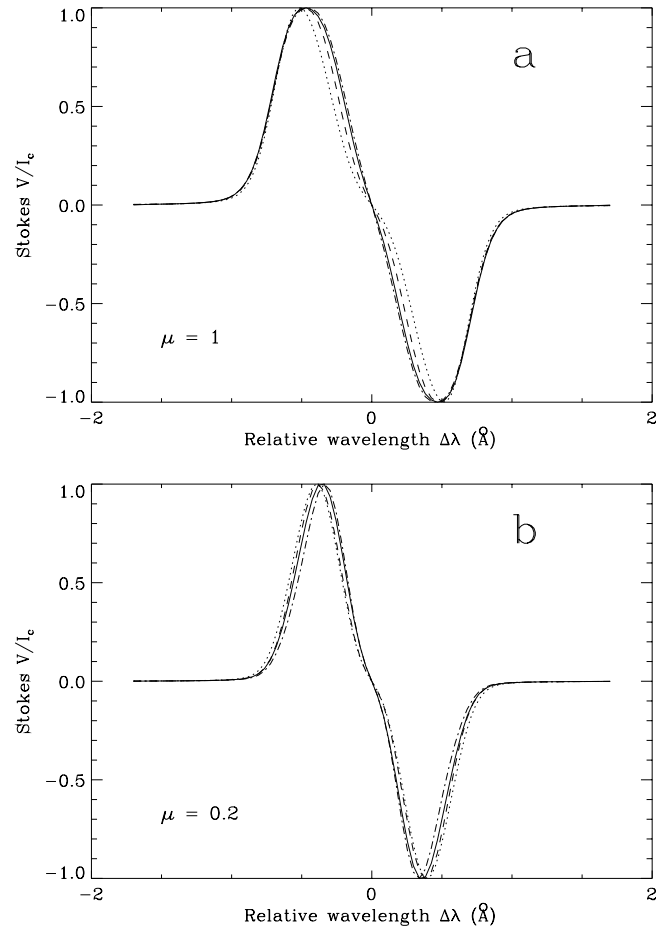


**Fig. 8a and b** Stokes  $V$  profiles of Fe I 15648 Å for models B, D, E and PLA. **a**  $\mu = 1.0$ , **b**  $\mu = 0.2$ . The profiles are broadened by 2 km s<sup>-1</sup>.

method may thus be an excellent technique for determining  $\langle B \cos \gamma \rangle$  at  $\mu = 1$ , but its reliability is reduced at smaller  $\mu$  for thin flux tubes. In spite of these problems, the c.g. method still provides more reliable results than the  $V$  amplitude or magnetographic observations. Another advantage of the c.g. method lies therein that it is insensitive to macrotrubulence or instrumental broadening. Thus Fig. 7 is also valid for broadened profiles.

### 3.7. The 15648 Å line

Fig. 8 shows  $V$  profiles of Fe I 15648 Å for models B, D, E and PLA at  $\mu = 1$  (Fig. 8a) and  $\mu = 0.2$  (Fig. 8b). Profiles due to the remaining models (C and G) are rather similar to those plotted and are not shown for clarity. The splitting at  $\mu = 0.2$  is 20–25% smaller than at  $\mu = 1$ , due to larger formation height near the limb, together with the vertical gradient of the field. The decrease of 15–25% between  $\mu = 1$  and 0.4 observed by Stenflo et al. (1987) is in rough agreement with the corresponding calculated decrease of 15–20% between  $\mu = 1$  and 0.4, which our models give.

According to Fig. 8 the Stokes  $V$  peak separation is almost independent of the flux-tube radius,  $R^*$ , unlike the findings of Zayer et al. (1989). We traced the difference to an insufficient

resolution of the flux tube boundary for the integration of the radiative transfer equation in the code employed by Zayer et al. (1989), which becomes most important for small flux tube radii. In the present work we have remedied the problem by using an adaptive mesh for that integration, as explained in Sect. 2.2.

We see little influence of the field-free atmosphere on the profile shapes of the 15648 Å line, in contrast to Fe I 5250.2 Å and 5247.1 Å; the inversion and flat portion in the cores of the visible Stokes profiles are absent in the infrared line (compare Figs. 2 and 3 with Fig. 8). This is partly due to the low formation height of the line. At this height the flux tube is cooler than its surroundings (i.e.  $I_\nu > B_\nu$  in the flux tube, so that no temperature inversion is produced). Furthermore, the 15648 Å line is relatively weak, unsaturated and temperature insensitive, all of which substantially reduces the absorption (and saturation) in the field-free part of the atmosphere. Finally, due to this line's large Zeeman sensitivity, its  $\sigma$ -components peak outside the wavelength range within which it absorbs in the field-free atmosphere. The  $V_{\max}(\mu)$  curves for the 2-D models (not shown) deviate correspondingly less from the plane-parallel case, compared to the visible lines. The counterparts of Figs. 4 and 7a for Fe I 15648 Å therefore also show correspondingly little scatter from one model to the next.

#### 4. Conclusions

We have tested a number of diagnostics of solar magnetic elements off disc centre. To this end we have calculated the centre-to-limb variation of Stokes profiles of three spectral lines in 2-D magnetohydrostatic models of flux tubes. Of the diagnostics considered here only the ratio of the amplitudes of Stokes  $V$  to the root mean square of  $Q$  and  $U$ , i.e.,  $V/\sqrt{Q^2 + U^2}$ , continues to give reliable results near the limb (in this case the inclination angle of the field). The rest of the diagnostics based on visible lines: the Stokes  $V$  amplitude, the centre-of-gravity technique and the Stokes  $V$  magnetic line ratio break down to a greater or lesser degree.

Probably the most important reason for this breakdown is that for near-limb observations, lines of sight pass through a sizeable amount of field free (or weak field) plasma in which absorption in the core of sufficiently strong lines (e.g. 5250.2 Å) may significantly influence their Stokes profiles. It affects profile shapes, Stokes amplitudes, line ratios, etc. Its influence on the profiles calculated here is particularly large, since we have used a relatively cool atmospheric model for the field-free atmosphere between flux tubes, in which the visible lines are significantly saturated.

We find that simple, plane-parallel models are quite adequate to determine the inclination angles of small magnetic flux tubes. Consequently, the analyses of Solanki et al. (1987), Sánchez Almeida & Martínez Pillet (1994), Bernasconi et al. (1995), Lites et al. (1993) and Bernasconi (1997) cannot be criticized in this respect. Caution is indicated if the magnetic field configuration has a sheet-like structure or if sunspot magnetic canopies are also present in the spatial resolution element (Solanki et al. 1996a).

The Stokes  $V$  amplitude decreases more rapidly for a flux tube with a finite diameter than for a plane-parallel model. For the atmospheres considered here, however, the 2-D models often lie closer to a simple  $V_{\max} \sim \mu$  scaling than the 1-D calculations. In 2-D models (again, for the atmospheric models used here) the magnetic line ratio (MLR) can attain values exceeding unity.

The CLV of Stokes  $V$  amplitude, area and  $I \pm V$  centre-of-gravity wavelengths provides an indication of the CLV of the magnetograph signal expected for vertical flux tubes. Our calculations suggest that at smaller  $\mu$  the magnetic flux is underestimated relative to  $\mu = 1$ . The centre-of-gravity method provides a somewhat better estimate than parameters like the Stokes  $V$  amplitude or the  $V$  value at a fixed wavelength.

There is another important point regarding the MLR. Since the value of the MLR depends sensitively on the angle between the flux-tube axis and the line of sight, an inclined thin flux tube near the centre of the solar disc should also give MLR values near unity (or possibly exceeding unity) even if it consists of a kG field. Such a line ratio would, using a simpler model, be suggestive of an intrinsically weak field. Observations at 15648 Å are, however, rather insensitive to this effect and should give unambiguous results.<sup>3</sup>

Finally, the current investigation reveals that the superiority of the Fe I 15648 Å line over Fe I 5250.2 Å as a probe of the magnetic field also extends to observations off solar disc centre. This underlines once more the need for a full-disc magnetometer operating on a daily basis in the Fe I 15648 Å line.

*Acknowledgements.* Thanks are extended to B. Lites for reading and commenting on the manuscript.

#### References

- Audic S., 1991, *Sol. Phys.* 135, 275
- Bernasconi P.N., 1997, *Stokes Vector Polarimetry: Observation and Analysis of Solar Magnetic Fields*, Ph.D. Thesis, ETH, Zürich
- Bernasconi P.N., Keller C.U., Povel H.P., Stenflo J.O., 1995, *A&A* 302, 533
- Briand C., Solanki S.K., 1995, *A&A* 299, 596
- Bruls J.H.M.J., Solanki S.K., 1993, *A&A* 273, 293
- Bruls J.H.M.J., Solanki S.K., 1994, *A&A* 293, 240
- Büntje M., Solanki S.K., Steiner O., 1993, *A&A* 268, 736
- Caccin B., Severino G., 1979, *ApJ* 232, 297
- Cauzzi G., Smaldone L.A., Balasubramaniam K.S., Keil S.L., 1993, *Sol. Phys.* 146, 207
- Chapman G.A., Gingell T.A., 1984, *Sol. Phys.* 91, 243
- Faurobert-Scholl M., 1992, *A&A* 258, 521
- Faurobert-Scholl M., 1994, *A&A* 285, 655
- Gingerich O., Noyes R.W., Kalkofen W., Cuny Y., 1971, *Sol. Phys.* 18, 347
- Grossmann-Doerth U., Pahlke K.-D., Schüssler M., 1987, *A&A* 176, 139

<sup>3</sup> The interpretation by Keller et al. (1994) of an MLR near unity in intranetwork elements as showing  $B < 500$  G, which can conceivably be due to inclined thin flux tubes with higher intrinsic field strengths is validated by the 15648 Å observations of Lin (1995) and Solanki et al. (1996b). These clearly show weak fields in intranetwork features.

- Grossmann-Doerth U., Schüssler M., Solanki S.K., 1988, *A&A* 206, L37
- Grossmann-Doerth U., Knölker M., Schüssler M., Weisshaar E., 1989, in *Solar and Stellar Granulation*, R.J. Rutten and G. Severino (Eds.), Kluwer, Dordrecht, p. 481
- Keller C.U., Solanki S.K., Steiner O., Stenflo J.O., 1990, *A&A* 233, 583
- Keller C.U., Deubner F.-L., Egger U., Fleck B., Povel H.P., 1994, *A&A* 286, 626
- Knölker M., Schüssler M., 1988, *A&A* 202, 275
- Knölker M., Schüssler M., 1992, in *Flux Tubes in the Solar Atmosphere*, E. Leer, P. Maltby (Eds.), *Inst. Theor. Phys., University of Oslo*, p. 17
- Knölker M., Grossmann-Doerth U., Schüssler M., Weisshaar E., 1990, *Adv. Space Res.* 11, 285
- Landi Degl'Innocenti E., 1976, *A&AS* 25, 379
- Lin H., 1995, *ApJ* 446, 421
- Lites B.W., Skumanich A., 1990, *ApJ* 348, 747
- Lites B.W., Elmore D.F., Seagraves P., Skumanich A., 1993, *ApJ* 418, 928
- Martínez Pillet V., Lites B.W., Skumanich A., 1997, *ApJ* 474, 810
- Ploner S.R.O., Solanki S.K., 1997, *A&A* 325, 1199
- Rees D.E., Semel M.D., 1979, *A&A* 74, 1
- Rees D.E., Murphy G.A., Durrant C.J., 1989, *ApJ* 339, 1093
- Ronan R.S., Mickey D.L., Orrall F.Q., 1987, *Sol. Phys.* 113, 353
- Rüedi I., Solanki S.K., Livingston W., Stenflo, J.O., 1992, *A&A* 263, 323
- Sánchez Almeida J., Martínez Pillet V., 1994, *ApJ* 424, 1014
- Sánchez Almeida J., Landi Degl'Innocenti E., Martínez Pillet V., Lites B.W., 1996, *ApJ* 446, 537
- Semel M.D., 1967, *Ann. Astrophys.* 30, 513
- Semel M., 1971, in *Solar Magnetic Fields*, R.F. Howard (Ed.), Reidel, Dordrecht, IAU Symp. 43, 37
- Solanki S.K., 1986, *A&A* 168, 311
- Solanki S.K., 1987, Ph.D. Thesis, No. 8309, ETH, Zürich
- Solanki S.K., 1989, *A&A* 224, 225
- Solanki S.K., 1993, *Space Sci. Rev.* 61, 1
- Solanki S.K., Keller C., Stenflo J.O., 1987, *A&A* 188, 183
- Solanki S.K., Steiner O., Uitenbroek H., 1991, *A&A* 250, 220
- Solanki S.K., Rüedi I., Livingston W., 1992, *A&A* 263, 312
- Solanki S.K., Finsterle W., Rüedi I., 1996a, *Sol. Phys.* 164, 253
- Solanki S.K., Zuffrey D., Lin H., Rüedi I., Kuhn J., 1996b, *A&A* 310, L33
- Spruit H.C., 1976, *Sol. Phys.* 50, 269
- Steiner O., 1990, Ph.D. Thesis, No. 9292, ETH-Zürich
- Steiner O., Pizzo V.J., 1989, *A&A* 211, 447
- Steiner O., Stenflo J.O., 1990, in *Solar Photosphere: Structure, Convection and Magnetic Fields*, J.O. Stenflo (Ed.), Kluwer, Dordrecht, IAU Symp. 138, 181
- Steiner O., Pneuman G.W., Stenflo J.O., 1986, *A&A* 170, 126
- Steiner O., Grossmann-Doerth U., Knölker M., Schüssler M., 1996, *Sol. Phys.* 164, 223
- Stenflo J.O., 1973, *Sol. Phys.* 32, 41
- Stenflo J.O., Harvey J.W., 1985, *Sol. Phys.* 95, 99
- Stenflo J.O., Solanki S.K., Harvey J.W., 1987, *A&A* 173, 167
- Van Ballegooijen A.A., 1985, in *Measurements of Solar Vector Magnetic Fields*, M.J. Hagyard (Ed.), NASA Conf. Publ. 2374, p. 322
- Walton S.R., 1987, *ApJ* 312, 909
- Zayer I., Solanki S.K., Stenflo J.O., 1989, *A&A* 211, 463